Adjognon, Guigonan Serge; Rivera-Ballesteros, Alexis; van Soest, Daniël Pieter

Article

Satellite-based tree cover mapping for forest conservation in the drylands of Sub Saharan Africa (SSA): Application to Burkina Faso gazetted forests

Development Engineering

Provided in Cooperation with:
Elsevier

Suggested Citation: Adjognon, Guigonan Serge; Rivera-Ballesteros, Alexis; van Soest, Daniël Pieter (2019) : Satellite-based tree cover mapping for forest conservation in the drylands of Sub Saharan Africa (SSA): Application to Burkina Faso gazetted forests, Development Engineering, ISSN 2352-7285, Elsevier, Amsterdam, Vol. 4, pp. 1-11, https://doi.org/10.1016/j.deveng.2018.100039

This Version is available at:
https://hdl.handle.net/10419/242297

Development Engineering 4 (2019) 100039

Contents lists available at ScienceDirect

Development Engineering

journal homepage: www.elsevier.com/locate/deveng

Satellite-based tree cover mapping for forest conservation in the drylands of Sub Saharan Africa (SSA): Application to Burkina Faso gazetted forests

Guigonan Serge Adjognon[1], Alexis Rivera-Ballesteros[*,1], Daan van Soest[2]

World Bank Group, 1818 H Street, NW, Washington, D.C., 20433, USA

ARTICLE INFO

Keywords:
Burkina Faso
Image classification
Forest cover
Sentinel-2
Google Earth engine
Sahel

ABSTRACT

While monitoring the effectiveness of forest conservation programs requires accurate data on (changes in) forest cover, many countries still lack the ability to map local forest inventory, especially in the drylands of Africa where forest areas are very sparsely covered. In this paper, we present a high resolution tree cover estimation of twelve gazetted forests in Burkina Faso using Random Forest-based supervised classification and Sentinel-2 satellite imagery sensed between March and April 2016. The methodology relies on ground truth sample points labeled manually over 10-m resolution images displaying a composite of near infrared (NIR), red and green bands extracted from Sentinel-2 multi-spectral satellite data to estimate tree cover with an average balanced accuracy rate of 80 percent. The output is a collection of rasters with binary values representing the combination of 10, and down-sampled 20 and 60-m bands indicating an estimate of the existence of trees or lack thereof, usable as a baseline for deforestation monitoring.

1. Introduction

Support for climate change mitigation policies has been mounting over the past two decades, both within countries as well as internationally. The loss of forest cover accounts for between 12 and 15 percent of the annual anthropogenic emissions of greenhouse gases – the second largest source after fossil fuel combustion (Canadell et al., 2007). Forest conservation is deemed to be a cost-effective way to mitigate climate change (Nabuurs, 2007). Not only are the opportunity costs of forest conservation relatively limited, there are also substantial co-benefits in the form of improved local climate regulation, better water storage, and biodiversity conservation (Canadell et al., 2007; Stern, 2007). Economic activities affecting loss of forest cover, especially in the drylands of Africa, include – but are not limited to – agricultural expansion, overgrazing, forest fires, demand for firewood and charcoal, over-exploitation of non-wood forest products, and mining (Griscom et al., 2017). In addition, the increasing need to grow food for a growing population around the world, coupled with the still widespread use of non-sustainable production practices, translates into increasingly serious forest degradation which threatens the livelihoods of both current and future generations. Halting deforestation has thus become a central objective in the climate policy of international agencies. A key example in point is the United Nations' initiative "Reducing Emissions from Deforestation and Forest Degradation" (REDD+) (Ministry of the Environment and Sustainable Development, Government of Burkina Faso, 2012). This initiative has gained wide popularity since the 2015 Paris Agreement, and several new countries have joined (or are preparing to join) this initiative.

Effective protection of forest resources requires detailed knowledge about the status of the resources, as well as the capacity to monitor changes. More importantly, the implementation of conservation policies such as payments for avoided deforestation, or the assessment of the impacts of forest conservation programs in general, demands the ability to regularly estimate – and as accurately as possible – the size of the resource stock as well as the changes therein. Global datasets of land cover, including tree cover, are now publicly available, including Global Forest Watch at 30 m resolution (based on Hansen et al., 2013), the ESA Land Cover CCI at 300 m; the Global Land Cover dataset at 30 m from China for 2000 and 2010; and Global, Landsat-based forest-cover change from 1990 to 2000 from Kim et al. (2014); for an overview, see Tsendbazar et al. (2014). Global land cover datasets are critical and cost-effective sources of information when national mapping capacity is not available yet. But national mapping is considered more accurate, as it can better account for the local circumstances (Global Forest Observation Initiative, 2014). Definitions of both land use and forest cover can vary largely with the context.

* Corresponding author.
E-mail address: ariveraballester@worldbank.org (A. Rivera-Ballesteros).
[1] Development Impact Evaluation (DIME), The World Bank Group (WBG).
[2] Department of Economics and Tilburg Sustainability Center, Tilburg University, the Netherlands.

https://doi.org/10.1016/j.deveng.2018.100039
Received 25 October 2017; Received in revised form 17 September 2018; Accepted 29 November 2018
Available online 30 November 2018

In this paper we present a low cost, easy to implement alternative approach to estimate forest cover relying on 10-m resolution Sentinel-2 imagery, highlighting the potential of large temporal and spatial capabilities using free publicly-accessible platform and data. This method will be especially useful for those countries that lack national mapping capacity to estimate their forest inventory, including many of the more arid countries in Africa. We leverage recent advances in satellite imagery technology to analyze large sets of images, and develop a land cover map for twelve Burkina Faso gazetted forests. The paper contributes to the available literature on satellite based image classification to map forest cover, especially in the drylands of Sub-Saharan Africa (SSA). We show the use of different spectral bands and remote sensing-derived indices to run a multi-spectral-based assessment at the pixel level, which is our spatial analysis unit. In addition, we present the accuracy metrics of our estimations at three different probability thresholds indicating how true positive and true negative rates change across them.

This research is implemented as part of DIME's impact evaluation support to the Forest Investment Program (FIP) in Burkina Faso, a targeted program of the Strategic Climate Fund set up under the Climate Investment Funds (CIF)[3] (Climate Investment Funds, 2014), from which Burkina Faso has benefited. The project includes the Gazetted Forest Participatory Management Project for REDD+ (PGFC/REDD+) financed through the African Development Bank (AfDB) (African Development Bank Group, 2013), which is aiming to conserve forest cover in Burkina Faso. The information provided in this paper will enhance Burkina Faso's ability to plan, implement and monitor the success of their FIP, and provide lessons for other countries in the region that are also part of the FIP initiative.

In this paper, we present tree cover estimates for the 12 gazetted forests in Burkina Faso that are targeted by the FIP project, between March and April 2016. The method used relies on a multi-spectral image classification at 10-m resolution, improving the prediction power, and therefore the mapping precision, compared to Landsat-based classifications. Sentinel-2 imagery contains thirteen spectral bands, four of which are sensed at a 10-m resolution: red, green, blue and near infrared (NIR) bands (European Space Agency, 2017). Goldblatt et al. (2017) have found that higher-resolution images improve the classification accuracy of ecosystems with relatively little tree crown cover, like forests in arid or semi-arid areas, which cannot be detected with Landsat imagery.

Image classification is performed using a random forest algorithm as classifier, as well as the Google Earth Engine (GEE) platform which combines a multi-petabyte catalog of satellite imagery and geospatial datasets with planetary-scale analysis capabilities allowing faster GIS and remote sensing computing. The general classification approach is based on the construction of a ground truth dataset that leverages on a false color composite image to label pixels with higher accuracy, and then uses a k-fold cross-validation approach to determine the probability of a trained pixel to be classified as tree-covered based on its spectral signature. The output is a collection of binary rasters that covers the total area of each one of the 12 gazetted forests of interest, indicating the existence of trees and displaying the accuracy rate of the results.

This paper is organized as follows. Section 2 describes the area of study indicating the agro-ecological characteristics of the forests of interest as well as the method and data used for the classification. Section 3 cover the calculations and the data construction process while section 4 presents the classification results. The fifth section concludes the paper with a discussion of the results.

[3] This research is part of DIME's impact evaluation support to the Burkina Faso's Forest Investment Program (FIP). Generous funding from the Climate Investment Fund (CIF) and the DIME-hosted i2i trust fund gratefully acknowledged.

2. Materials and methods

2.1. Study context

Burkina Faso is a landlocked country in West Africa, located in the drylands of Sub Saharan Africa (SSA), between the Sahara Desert and the Gulf of Guinea (Bastin et al., 2017). Most of the country belongs to the Sahel region, with semi-arid climatic conditions, considered as the transition between the Sahara and the Sudanian Savanna with vegetation dominated by shrubs and steppe (United States Geological Survey, 2016). The southern part of the country is the transition between the Sahelian and Sudanian climates characteristic of a tropical savanna. While the north receives an average rainfall of 300–400 mm per year, the south is a more humid area that receives an average annual amount of rainfall of 650–1000 mm and is irrigated by permanent rivers (United States Geological Survey, 2017). As defined by Fontès and Guinko (1995), Burkina Faso's agro-ecological zoning distinguishes four main phytogeographical zones: (from north to south) North Sahelian, South Sahelian, North Sudanian, South Sudanian (Fig. 1). While the North Sahelian is the most arid part of the country, the South Sudanian is benefited by more abundant rainfall and greener vegetation. The North Sudanian and the South Sahelian are the transition between the other two zones and show distinct climate conditions, thus the density and phenological patterns between them varies.

Burkina Faso is implementing a FIP-funded forest conservation program targeting 12 out of 77 gazetted forests, with the assistance of the African Development Bank (AfDB) and the World Bank Group (WBG). The forest classification analyses in this paper focus on those 12 forests, and the output offers a benchmark against which the effectiveness of forest conservation projects can be assessed in the future. Table 1 and Fig. 2 present the 12 gazetted forests targeted by the Burkina Faso FIP, where the majority of them (eight) are located in the North Sudanian and the other four in the South Sudanian.

2.2. Leveraging recent advances in remote sensing technology

The recent advances in satellite imagery and processing technology have improved the availability of low to no cost satellite images, at sufficiently high temporal and spatial resolutions. This has, in turn, pushed the boundaries of forest observation capacities, allowing the development of global land cover mappings of relatively medium to high resolution to allow cost effective forest monitoring. Likewise, new cloud-based platforms such as GEE have provided capability for storing petabytes of satellite images at a global scale, and algorithms for supervised image classification, with free access for research purposes. These advances allow the collection and processing of data at a much larger scale and at higher accuracy even in relatively inaccessible areas and in regions with insufficient data collection capacity.

Until now, the most commonly used tool to (Hansen et al., 2007). This dataset relies on Landsat imagery, and is useful to estimate changes of forest cover especially in densely forested regions (Churches et al., 2014). It has been used in several studies to evaluate the impact of forest conservation policies (e.g. Blankespoor et al. (2017)). A popular application of the Hansen dataset is the Global ForestWatch, a joint effort from different organizations to make forest cover layers readily available via an easy-to-use tool (University of Maryland, 2015).

While other global-scope land cover products (i.e. (Hansen et al., 2007), (Tsendbazar et al., 2014)) are available, these products trade global coverage for local accuracy in some contexts (Mitchard et al., 2015). We build on these global approaches by leveraging similar approaches in a localized context to create a land cover m quantify forest change globally is the Hansen's dataset developed using time-series analysis of Landsat images. This dataset has been published in three versions which are updated yearly since its first publication in 2013ap for Burkina Faso, providing improved temporal and spatial resolution.

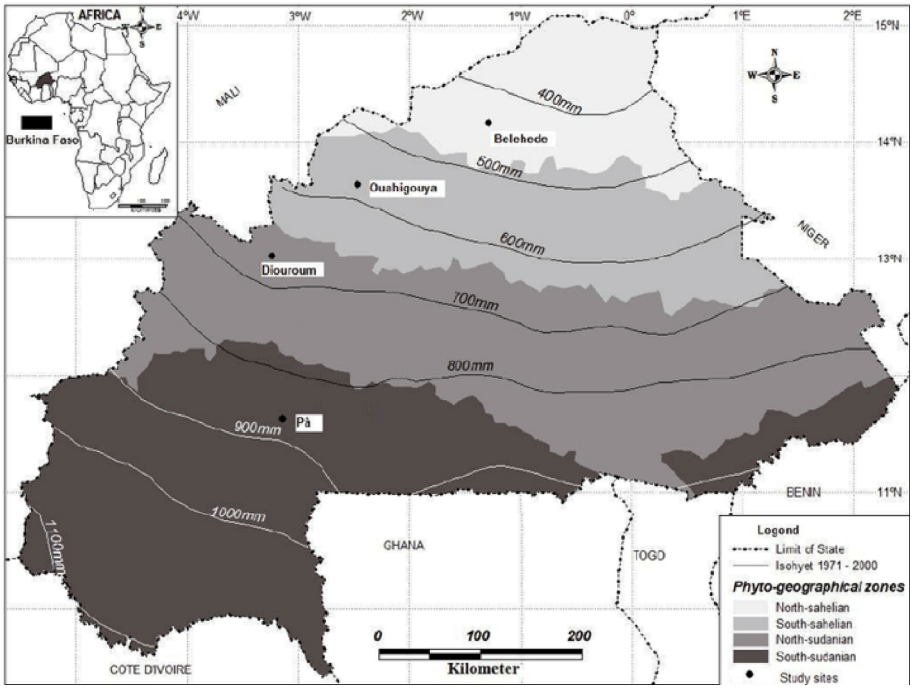

Fig. 1. Agro-ecological zones in Burkina Faso. Source: Bognounou et al. (2010).

Table 1
Forests participating in the Forest Investment Program (FIP) with their agro-ecological zones.

Forest	Agro-ecological zones	Name
1	South Sudanian	Bontioli Gazetted Forest (Total Reserve)
2	South Sudanian	Bontioli Gazetted Forest (Partial Reserve)
3	North Sudanian	Tissé Gazetted Forest
4	North Sudanian	Sorobouli Gazetted Forest
5	South Sudanian	Sylvo-pastoral Zone of Tapoa - Boopo
6	North Sudanian	Toroba Gazetted Forest
7	South Sudanian	Nazinon Gazetted Forest
8	North Sudanian	Kari Gazetted Forest
9	North Sudanian	Tiogo Gazetted Forest
10	North Sudanian	Ouoro Gazetted Forest
11	North Sudanian	Koulbi Gazetted Forest
12	North Sudanian	Nossebou Gazetted Forest

2.3. Sentinel-2 imagery

The European Sentinels consist of a fleet of satellites dedicated to providing imagery for Earth observation purposes. Sentinel-2 is part of the European Commission's Copernicus program and provides higher multispectral resolution with 13 bands that help to monitor variability in land surface conditions over large areas every 10 days (European Space Agency, 2015).

This mission supports Copernicus environmental studies that include monitoring of vegetation, soil, water and coastal areas. Amongst Sentinel-2 bands, blue (band 2), green (band 3), red (band 4), RGB, and NIR (band 8), are available at a 10 m resolution (European Space Agency, 2015). The other bands are available at 20-m or 60-m resolutions. These images are freely accessible to the public, and hence represent a low-cost solution for Earth observation and image processing at higher temporal and spatial resolution and with multispectral information.

2.4. Ground truth training dataset construction

This study uses Sentinel-2 imagery with bands of spatial resolution that range from 10 to 60 m, facilitating the detection of forest covered areas that may be imperceptible to lower resolution imagery such as Landsat. It offers an alternative for tree cover classification without the need for expensive very high-resolution images. The strategy in this paper for mapping tree cover is based on supervised classification that uses ground truth labels. Our approach was as follows.

First, we selected the images from the Sentinel-2 image library that were suitable for the creation of ground truth data. For this, we filtered images with least cloud cover in 2016 found between March and April, coinciding with Burkina Faso's dry season. Since Sentinel-2 imagery comes with 13 spectral bands, it is possible to use different color combinations to facilitate the visual detection of tree cover in the study area. Using the combination of red, green and blue color bands, the contrast between tree cover and other types of land cover is relatively low, and hence it is hard to determine the location of trees from simple visual appreciation. Instead, we used the combination of the NIR band, color red and color green to generate a color composite known as false color. The false color composite shows trees in brighter color red contrasting with darker and lighter colors of other types of land cover. However, as evidenced by Fig. 3, this composite still does not allow for accurate detection of the differences between the various types of non-tree land cover.

Second, we created four 100-square kilometer polygons of equilateral square shape across the 12 project forests, capturing as much as possible the variation in agro-ecological conditions (Fig. 4). Inside each square polygon, a total of 1000 ground truth points were randomly selected, and coded manually using visual interpretation, to serve as ground truth data. The 4000 ground truth points were displayed overlaying a Sentinel-2 image where each point falls into a 100-square kilometer polygon. We manually assigned a value of '0' if that pixel visually did not have the characteristics of a tree pixel and a value of '1' if the pixel has tree characteristics (see Fig. 5). We decided to not include other classes of land cover to remain consistent with our original goal which focuses primarily on tree cover mapping in forests areas as opposed to land cover mapping generally. In addition, we found, in our areas of interest, that the pixels that cover built-up areas and water bodies were too few to include them in the classification algorithm – not very surprising, as these are gazetted forests. While Sentinel-2

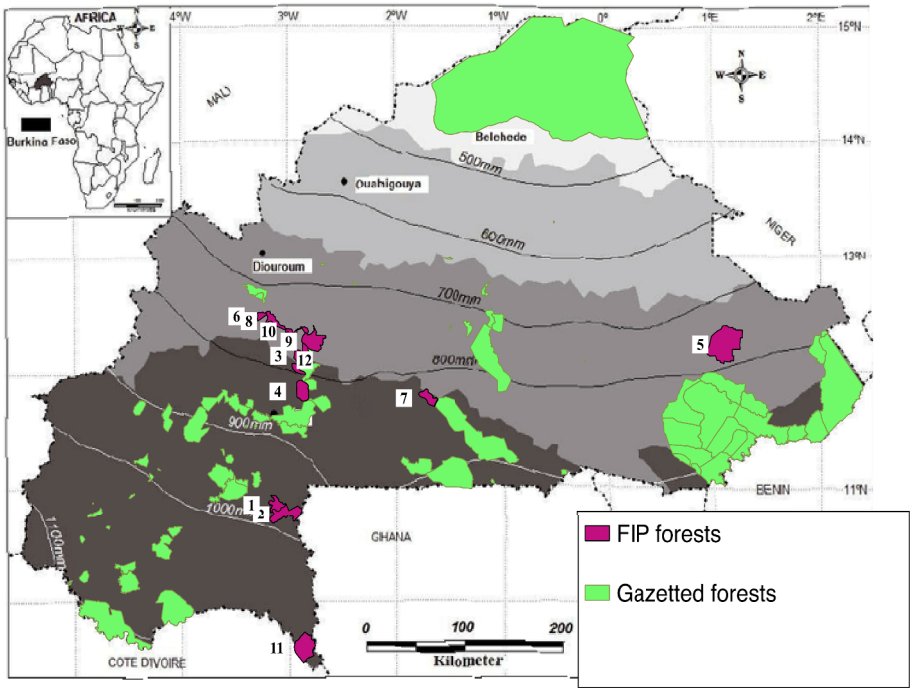

Fig. 2. The locations of the gazetted forests in Burkina Faso, including the 12 FIP forests.

images show distinguishable patterns between different types of crops in other regions of the world (Belgiu and Csillik, 2018), in this case are not so evident. Since our assessment only considers the winter season when soil and moisture is significantly lower, crop fields that do not depend on an irrigation system (that is most of the cases in this area) reflect a very similar spectral signature to the surrounding vegetation. In addition to this, most of the gazetted forests show a lower agricultural activity, resulting in a low percentage of crop field ground truth points compared to other land cover classes.

2.5. Classification assessment

Every Sentinel-2 image consists on 13 spectral bands the combination of which results in a spectral signature for each pixel. RGB bands create color contrasts between different types of land cover that a naked eye can distinguish and these bands represent an important part of the pixel's spectral signature. However, using only the RGB would limit the wavelength range of our classification method from 0.45 to 0.69 μm, while the full range of the wavelength reflected from the surface could reach up to 2.5 μm using the remaining bands available on these images (European Space Agency, 2015). For example, the NIR (0.7 μm–0.9 μm) band provides information about the greenness of the reflected surface which helps us to identify live and healthy vegetation, while the shortwave infrared (SWIR) (0.9–2.5 μm) bands provide information about the water content of the surface being useful to differentiate dry bare land from wet soils where vegetation is more likely to exist (Davison et al., 2006). Furthermore, their higher wavelengths are less affected by atmospheric disturbances and are used to build indices that are used to detect vegetated and non-vegetated land cover. In addition to these bands, we use three bands with 60 m spatial resolution: aerosols (band 1), water vapor (band 9) and cirrus (band 10). They provide data that is not reflected from the surface but they do provide relevant information for atmospheric corrections. While we selected images with low percentage of cloud cover during Burkina Faso's dry season, smaller clouds and airborne particles formed by evaporation, fires, pollution, etc. could be affecting the absorption of sunlight and therefore the reflectance values of the bands' wavelengths. The information from these bands is included as part of the prediction input to add data from unobserved patterns that might be affecting the other bands reflectance values. These are also rescaled to the resolution of the classification output (10 m) using the nearest neighbor method.

The Sentinel-2 image bands can be used to calculate indices that are able to capture specific types of land cover, and are especially useful for detecting (changes in) vegetation and soil (Pesaresi et al., 2016). Puletti et al. (2018) have found that including vegetation indices to the machine learning algorithm produce better classification results compared to those obtained when it's only used the simple images, therefore we have calculated and included the following:

- Normalized difference vegetation index (NDVI): reflects the relation between red visible light (RED, which is typically absorbed by a plant's chlorophyll) and NIR wavelength (which is scattered by the leaf's mesophyll structure) (Glenn et al., 2008). The NDVI is calculated as (NIR-RED)/(NIR + RED);

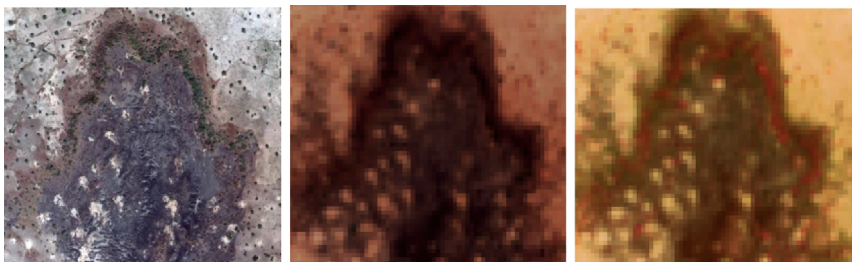

Fig. 3. Sentinel-2 10-m resolution using RGB band combination vs false color combination (NIR, red and green) for a sylvo-pastoral zone in the Tapoa Boopo forest. From left to right: a) shows Google high resolution basemap as a visual reference, b) shows the Sentinel-2 RGB image and c) shows the Sentinel-2 false color image. The Sentinel-2 images were obtained in March 2016. (For interpretation of the references to color in this figure legend, the reader is referred to the Web version of this article.)

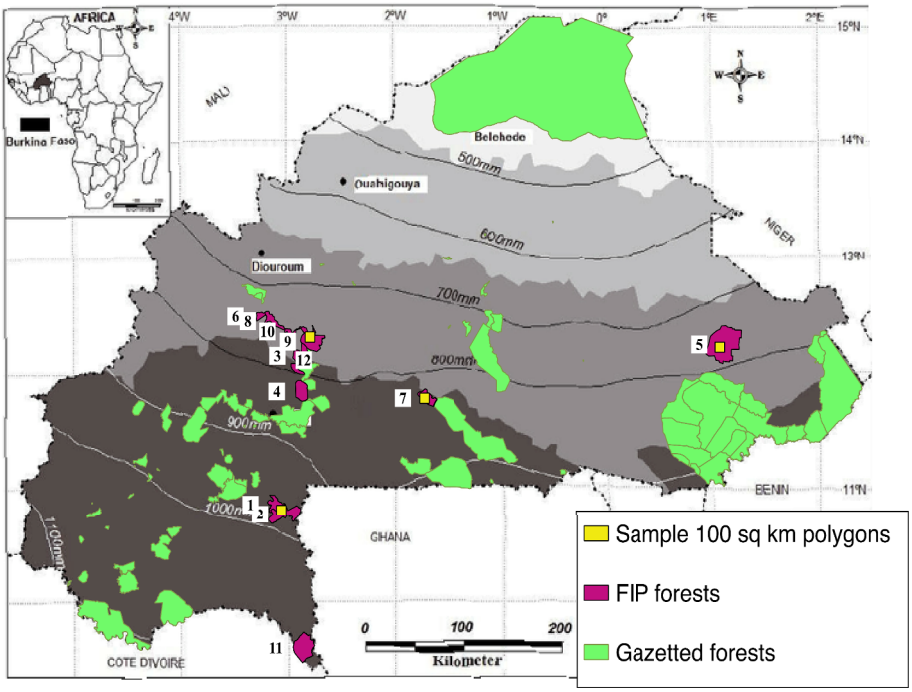

Fig. 4. Identification of four 100-square kilometers. polygons within the 12 project forests, taking into account the geographic distribution of the country's gazetted forests, the various agro-ecological zones they are located in as well as their latitudes, to account for differences in ecosystems across the country.

- Normalized difference water index (NDWI): captures the amount of water present in leaf internal structures and is useful to detect water bodies (Gao, 1999). Short wave infrared (SWIR, with wavelengths between 1400 and 2400 nm) is absorbed by water, and hence can be used to detect the presence of soil in plants. The NDWI is calculated as (NIR-SWIR)/(NIR + SWIR);
- Normalized difference built index (NDBI): captures the relation between the SWIR and the near infra-red wavelengths (Zha et al., 2013). Contrasting the other indices where the NIR band appears with a positive sign in the numerator, here it is subtracted showing higher values in areas with low vegetation. The index assumes a higher reflectance of built-up areas in the medium infra-red wavelength range than in the near infra-red. In forests like Bontioli, where small built-up areas can be found, the NDBI will give additional information to confirm that those pixels should not be classified as non tree cover. It is calculated as: (SWIR-NIR)/(SWIR + NIR);
- Enhanced vegetation index (EVI): index that improves sensitivity in high biomass regions reducing the atmosphere influences, especially in areas of dense canopy which uses the blue band to correct aerosol influences in the red band, showing photosynthetically active vegetation (Huete et al., 1994, 1997, 2013). It is calculated as: G * ((NIR - RED)/(NIR + C1 * RED - C2 * BLUE + L)), where coefficients are adopted from the MODIS-EVI algorithm indicating the gain factor (G = 2.5), the adjustment for correcting differential, red radiant and non-linear transfer through canopy (L = 1), and the aerosol resistance term which corrects atmospheric influences in the red band (C1 = 6 and C2 = 7.5). EVI adjustments are designed to make EVI more robust than NDVI in areas with high soil exposure and in dense vegetation, but also more sensitive than NDVI to variation in the viewing geometry, surface albedo, and sun elevation angle across variable terrain (Garroutte et al., 2016). However, there are some existing scientific controversies that question the use of EVI (Morton et al., 2014; Saleska et al., 2007), therefore we

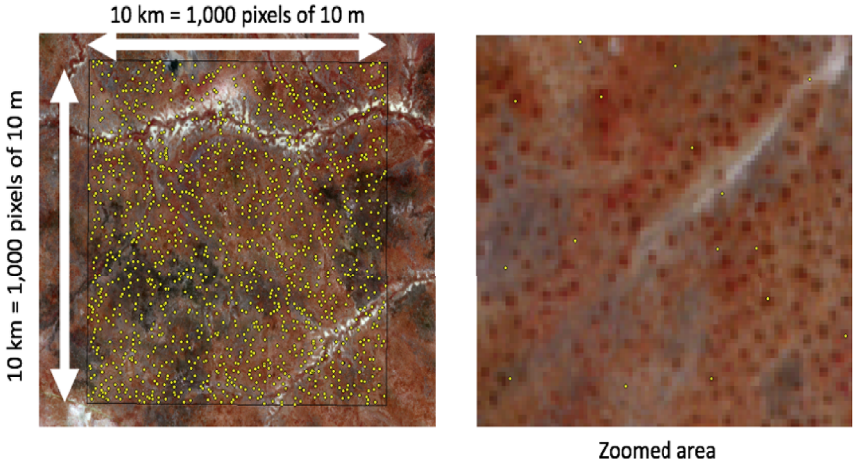

Fig. 5. Ground truth dataset created from random points overlying Sentinel-2 images where tree covered pixels are identified with a brighter color red. (For interpretation of the references to color in this figure legend, the reader is referred to the Web version of this article.)

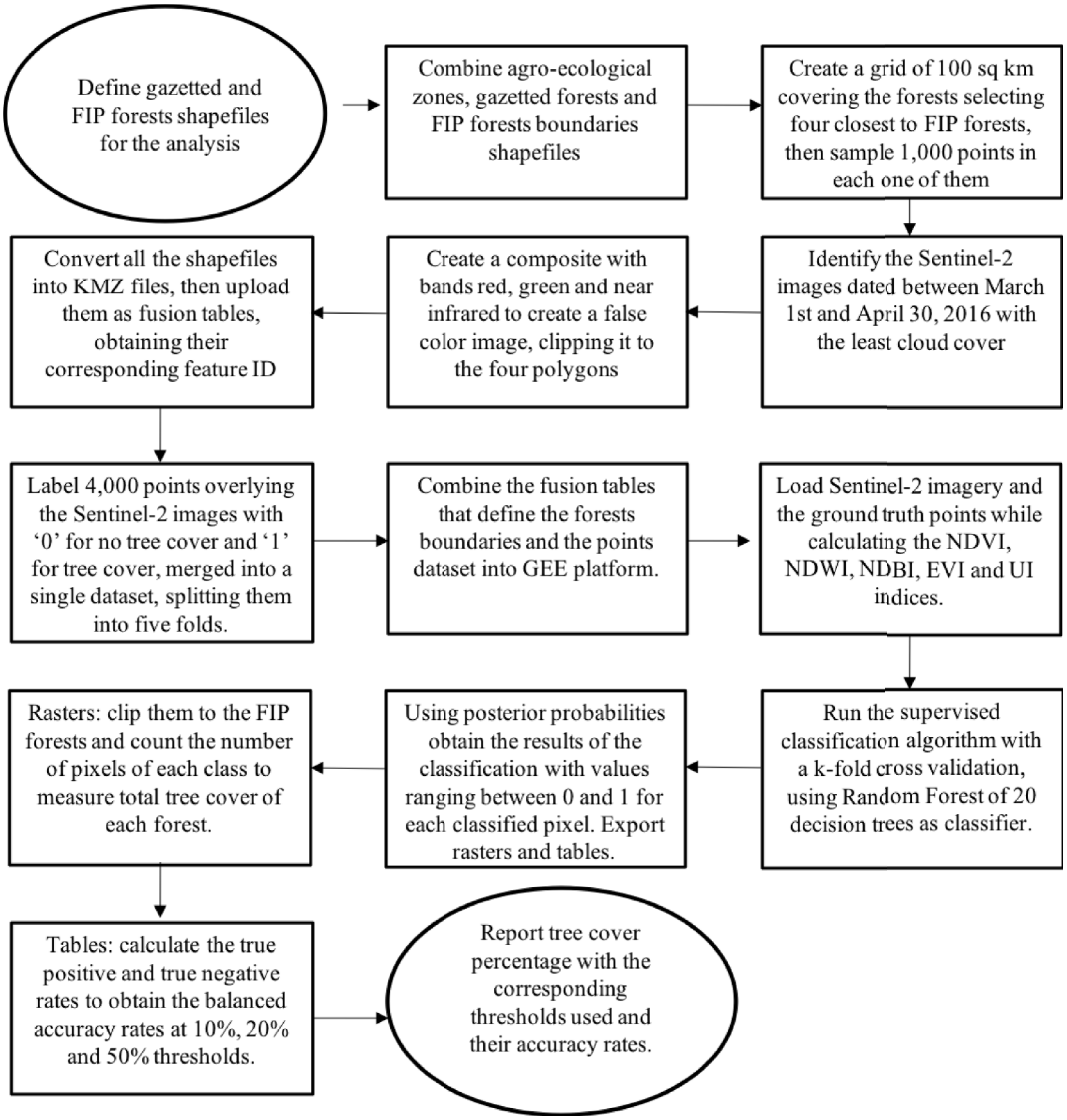

Fig. 6. Methods flowchart. This flowchart shows in 14 steps how we estimated forest cover for each FIP forest from raw satellite imagery and simple vector data defining areas of study.

decided to also include NDVI, an index that has been widely used in remote sensing and classification algorithms, for example: Puletti et al. Puletti et al. (2018); Goldblatt et al. (2016, 2017). The inclusion of these two indices that are highly correlated, does not affect the model's prediction power and results, since Random Forest classifier is a nonlinear algorithm (Breiman, 2001) and these are less affected by multicollinearity (Morlini, 2006; Feng et al., 2018);

- Urban index (UI): measures the density of man-made constructions where higher values indicate a higher built-up intensity area (Kawamura et al., 1996). It is calculated as: (SWIR2 - NIR)/(SWIR2 + NIR). The SWIR2 band corresponds to the short-wave infrared with a wavelength between 2107 nm and 2294 nm that represent the highest wavelength values of Sentinel-2 bands which are reflected when some minerals like metals appear. Therefore, when SWIR2 values are higher relative to NIR values, this typically means that the pixel lacks vegetation and contains more built-up areas, similar to how the NDBI works. The inclusion of the NIR is helpful to identify areas with no vegetation as the NDBI does, but with the SWIR2 band, reflectance with higher bandwidths will be captured. Using this index, a larger bandwidth spectrum is covered, adding information to detect possible patterns of more types of land cover that should not be classified as tree cover.

While RGB and NIR are sensed at a 10 m resolution, the short wave infrared bands (SWIR1 and SWIR2) are available at a 20 m resolution. To address this spatial resolution difference, the pixel values with lower resolution are re-sampled to fit the 10 m resolution using the nearest neighbor method. The classification assessment consisted in dividing the ground truth data randomly into five folds to perform a k-fold cross validation that could use four folds to train the pixels and one fold to test the accuracy of the results (Fisher et al., 2017). That means that each set of ground truth points for each fold inside a sample polygon was used four times as a training point and one time as a test point.

Because the methodology relies on a supervised classification method, we needed to find an adequate classifier to train and classify pixels. A classifier is a collection of condition-action rules used in learning systems (Lanzi et al., 2018). Classifiers can be found in two types: parametric and non-parametric. A parametric classifier is based on the statistical probability distribution of each class and relies on the statistical data of samples. A non-parametric classifier is used to estimate the probability of unknown density functions, such as those used in machine learning (Kumar and Sahoo, 2012). There are a number of classification algorithms that we could use for our classification. Since the purpose of this work is not to test the differences between different classifiers, we rely on previous studies that have used different

Table 2
Accuracy metrics for the training and testing datasets inside the four polygons used for classification.

	Threshold = 0.1		Threshold = 0.2		Threshold = 0.5	
P1	TPR	0.97	TPR	0.92	TPR	0.82
	TNR	0.41	TNR	0.64	TNR	0.84
	Balanced	0.69	Balanced	0.78	Balanced	0.83
	Threshold = 0.1		**Threshold = 0.2**		**Threshold = 0.5**	
P2	TPR	0.98	TPR	0.92	TPR	0.78
	TNR	0.29	TNR	0.52	TNR	0.78
	Balanced	0.63	Balanced	0.72	Balanced	0.78
	Threshold = 0.1		**Threshold = 0.2**		**Threshold = 0.5**	
P3	TPR	0.97	TPR	0.93	TPR	0.83
	TNR	0.42	TNR	0.61	TNR	0.82
	Balanced	0.69	Balanced	0.77	Balanced	0.83
	Threshold = 0.1		**Threshold = 0.2**		**Threshold = 0.5**	
P4	TPR	0.97	TPR	0.93	TPR	0.8
	TNR	0.33	TNR	0.55	TNR	0.77
	Balanced	0.65	Balanced	0.74	Balanced	0.78
	Threshold = 0.1		**Threshold = 0.2**		**Threshold = 0.5**	
Avg	TPR	0.97	TPR	0.92	TPR	0.81
	TNR	0.36	TNR	0.58	TNR	0.80
	Balanced	0.67	Balanced	0.75	Balanced	0.80

classification algorithms to run similar experiments. Goldblatt et al. (2016) tested three different classifiers to classify land cover: (i) the Classification and Regression Tree classifier (CART); (ii) the Support Vector Machine classifier (SVM); and (iii) the Random Forest classifier. Belgiu and Dragut (2016) have tested the Random Forest classifier in remote sensing and found that it successfully handles high data dimensionality and multicolinearity, being both fast and insensitive to overfitting (Belgiu and Dragut, 2016). Goldblatt et al. (2017) have also used Random Forest to classify tree cover in Brazilian semiarid ecosystems with similar results and Puletti et al. Puletti et al. (2018) have reached an accuracy rate of 83% when using Random Forest to map types of forest cover in the Italian Mediterranean. A Random Forest classifier is a supervised learning method that uses kernel functions (vectors within matrices) to define vector parameters of the data producing multiple decision trees, using a randomly selected subset of training samples and variables (Belgiu and Dragut, 2016). In practice, the method consists of a decision-tree classifier that includes k-decision trees (k-predictors) (Cutler et al., 2012; Karlson et al., 2015) When classifying an example, the example variables are run through each of the k tree predictors, and the k predictions are averaged to get a less noisy prediction (by voting on the most popular class). The learning process of the forest involves some level of randomness; each tree is trained over an independent random sample of examples from the training set and each node's binary outcome in a tree is determined by a randomly sampled subset of the input variables (Rodriguez-Galiano et al., 2012).

3. Calculations

The overall method flowchart used in this paper is summarized in Fig. 6. Our ground truth dataset consists of 4000 ground truth points. Using this ground truth data and the classifier described above, we trained all pixels within each of the 12 FIP forests. The pixel-based classification method used the thirteen spectral bands of Sentinel-2 imagery plus the five indices explained above. The number of trees used for Random Forest classifier was determined based on Goldblatt et al. (2016, 2017). Goldblatt et al. estimated the average accuracy that resulted from using 1, 3, 5, 10, 50 and 100 decision trees. They found that on average, accuracy was highest when using between 10 and 50 decision trees. Based on this evidence, we also decided to use 20 decision trees for our assessment.

The classification algorithm was applied not only to the area inside the sampled square polygon, but it was also extrapolated to the rest of the area within the FIP forests, assuming that neighboring forests have homogeneous land cover patterns given the proximity to the sampled area and their location within the same agro-ecological zone.

To estimate the accuracy of the supervised classification algorithm we use a k-fold cross validation where in each experiment, four folds are used as training dataset and the remaining fold is used as the testing fold. The experiment is run five times where each fold works as the testing dataset. To calculate the accuracy metrics of our assessment, we used posterior probabilities to assign a continuous value between '0' and '1' to each pixel, which represents the conditional probability of taking a certain value based on the spectral signature of the pixel -– the more vegetation the pixel has, the higher the value the posterior probability will be (Goldblatt et al., 2016; McRoberts et al., 2014). Since treetops might not be big enough to fully cover the area of a Sentinel-2 pixel and the number of tree cover pixel training samples is much lower than the number of sample pixels without tree cover, the likelihood of a pixel to be classified as having no tree cover is higher. Therefore, the lower the probability of being classified as tree cover, the higher the true positive rate will be. Using a one hundred percent posterior probability classification would result in very few rates of true positives.

Since we used the method of posterior probabilities, the output of this algorithm is an image formed by pixels where each one has a value between '0' and '1' representing the likelihood of being classified as tree or non-tree covered. Then, we defined thresholds to determine the estimated binary value of each pixel observation. We selected the threshold values of 10 percent, 20 percent and 50 percent to observe how true negative and true positive rates behave.

At the same time, we produced a table indicating the labeled value of the test set of points and the predicted value of those same points based on the classification algorithm. These were used to calculate accuracy metrics of the classification focused on sensitivity and specificity. The sensitivity evaluates how good the model is at predicting true positives (similar to the type I error in statistics), while the specificity estimates show how likely it is to have a false negative (akin to a type II error) (Wang et al., 2010). Table 2 summarizes the accuracy metrics based on the three thresholds. Overall, the 10 percent threshold generated the highest true positive rates (TPR) in these forests but also generated the lowest rates of true negatives (TNR). As thresholds increased, true positive rates dropped but true negative rates went up, resulting in higher balanced accuracy rates (BAR = [TPR + TNR]/2). These outcomes suggest that isolated trees have a canopy smaller than the Sentinel-2 pixel size and provide lower values for vegetation of the pixel spectral signature. Furthermore, the lowest threshold will result in the highest true positive rates and the highest threshold will result in the highest true negative rates, but in both cases the balanced accuracy rate will be smaller than setting a 0.5 threshold. We used the raster with the classified image displaying the classification results from the three different thresholds used. Then, these rasters allowed us to calculate the number of pixels that represent forest cover under that threshold and exported the classified image to a map.

4. Results and discussions

Our analysis yielded twelve classified images corresponding to the twelve FIP forests of interest. The resulting raster dataset shows the pixels classified as tree cover using the 10, 20 and 50 percent thresholds. Fig. 7 shows an example of the pixels from the rasters representing tree cover in Tissé Forest using the three different posterior probability threshold values used for the output of the classification. We can observe that as we increase the threshold, the number of pixels classified as tree cover decreases and some smaller tree tops might be not detected. However, using lower thresholds, the number of pixels classified

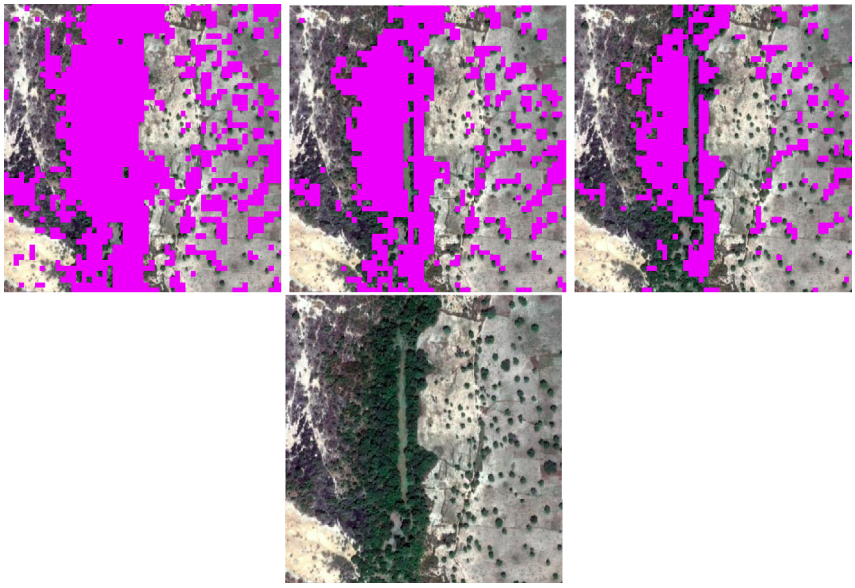

Fig. 7. Comparison between different threshold outputs. This image shows a zoomed sample in Tissé Forest with centroid −2.889619, 12.170764 showing tree cover pixels obtained from our image classification method using the three different threshold outputs over a high resolution image. On the top row from left to right: 0.1, 0.2 and 0.5 thresholds. On the bottom row we show the high-resolution image used as background for comparison purposes.

as tree cover increases, but this might be leading to some extent of misclassification. Therefore, the optimal threshold to use as the classification output, will depend on the trade off between the true positive rate and the balanced rate.

We estimated the total tree-covered area by summing the areas of the pixels classified as 'tree cover' using the 10 percent, 20 percent and 50 percent threshold. We then calculated the share of tree cover area in the total forest area. The results for each forest, are presented in Table 3 and in Figs. 8–10.

The output rasters were also exported as a KML file to Google Fusion tables to present the full estimated forest cover classification using the lowest threshold.

We found that the estimation of tree cover with relatively low tree canopy density can be mapped at a low cost using satellite images and cloud-based platforms. The resulting average balanced accuracy rates are 0.67, 0.75 and 0.8 depending on the posterior probability thresholds used as output from a Random Forest-based classification.

5. Conclusions

Monitoring progress towards REDD + requires a better ability for government to monitor forest cover, and track changes resulting from various programs. In attempt to generate forest cover datasets better tailored to the specific conditions of the drylands, we provided a new estimation of forest cover using higher resolution satellite images, in combination with ground truth points carefully labeled inside the area of interest.

We have demonstrated the opportunity for taking advantage of higher resolution and freely available Sentinel-2 satellite images to map forest cover in the drylands, using twelve FIP focused Burkina Faso forests as an example for the period covering March–April 2016. Higher resolution imagery such as Sentinel-2 provide a low-cost approach to map tree cover in these special agro-ecological conditions.

However, this study is subject to some limitations. First, while the 10 m Sentinel-2 images used are of higher resolution than other satellite images, the classification derived from them is still not perfect. For example, tree tops could measure as small as 3 m of diameter and since we are using bands with resolutions ranging from 10 to 60 m, these could remain undetected by our classification algorithm. Second, while using Sentinel-2 imagery to label the ground truth points, we used visual interpretation and labeled manually 4000 points, exposing the ground truth data to potential human error due to fatigue or misinterpretation. This has also limited the number of points that we could label and use as ground truth. Future possibilities may include crowdsourcing this activity through online platforms integrating GIS capabilities. This would allow for more flexibility in our sampling strategy, using enough ground truth points, and capturing enough of the spatial variability in spectral signature in the areas of interest.

Finally, using the Random Forest classifier, we performed the classification using 20 trees based on the results of other studies (Goldblatt et al., 2016). For future research, we propose to use an accuracy assessment using different number of trees and test for the optimal number of trees needed for this specific area altogether with a k-fold cross validation where the division in folds of the data into training sets and test sets will produce statistics about how accurate the classifiers are.

Extension of this work would include the remaining 55 gazetted forests of Burkina Faso, for a more comprehensive monitoring of forests resources in Burkina Faso. It will also use higher resolution images from tasked satellites or drone images to improve ground truth labeling that could increase the precision of the training data used for the classification. This method should then be incorporated into a routine forest monitoring system allowing Burkina Faso's government to track in real time changes in forest resources and evaluate the outcomes of conservation programs. Several other countries in the Sahel regions could also adopt this approach for a consistent progress towards reduced deforestation in the Sahel region.

Table 3
Image classification results using the threshold of 0.5

Forest	Forest name	No tree cover %	Tree cover %	Total area (has.)
1	Foret,Classée de Bontioli (R. Totale)	59.22	40.78	14,146.88
2	Foret,Classée de Bontioli (R. Partielle)	73.41	26.59	33,816.16
3	Foret Classée de Tissé	59.08	40.92	20,863.17
4	Foret Classée de Sorobouli	75.10	24.90	21,155.34
5	Zone sylvo-pastorale Tapoa - Boopo	65.12	34.88	87,842.02
6	Foret Classée de Toroba	46.92	53.08	4719.88
7	Foret Classée du Nazinon	54.93	45.07	15,166.93
8	Foret Classée de Kari	65.18	34.82	11,659.07
9	Foret Classée de Tiogo	63.95	36.05	30,785.28
10	Foret Classée de Ouoro	63.77	36.23	7461.86
11	Foret Classée du Koulbi	84.58	15.42	40.832.49
12	Foret Classée de Nossebou	78.27	21.73	6557.53

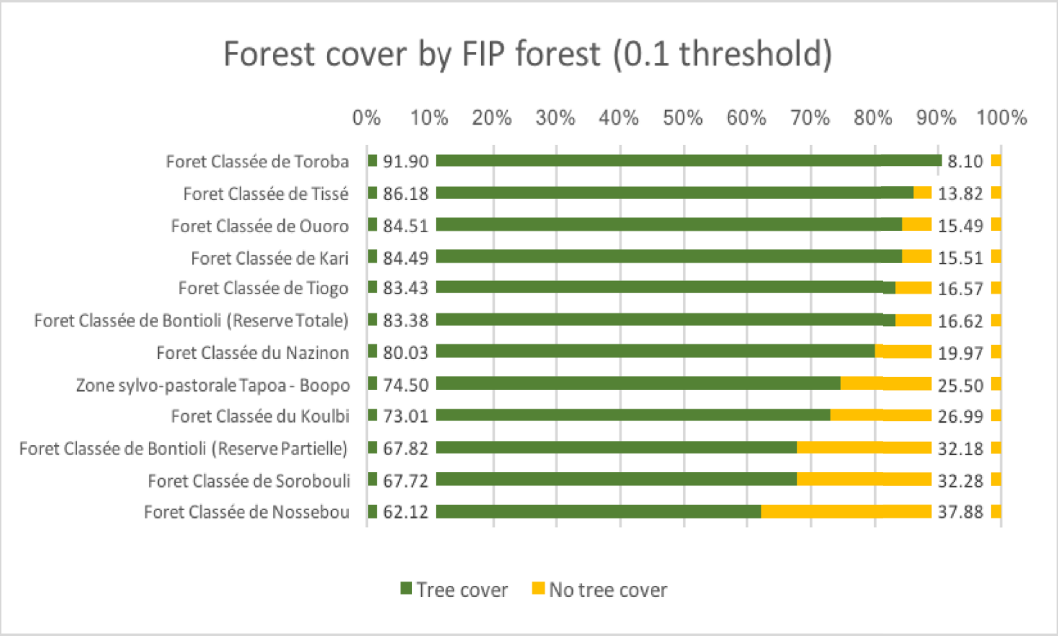

Fig. 8. Forest cover by gazetted forest for 0.1 threshold.

6. Glossary

ArcMap: is a geographic information system (GIS) software developed by Esri for working with maps and geographic information.
Basemap: Map provided by software applications to show an image of the area observed for visual appreciation.
Classifier: A machine learning method to assign values to a set of observations given their attributes.
GEE: Google Earth Engine is an online platform that leverages cloud-computational services for planetary-scale analysis and consists of petabytes of geospatial and tabular data, including a full archive of Landsat scenes, together with a JavaScript, Python based API (GEE API), and algorithms for supervised image classification.
KML: a keyhole markup language file is an XML notation for expressing geographic annotation and visualization within Internet-based developed by Google Earth.
Landsat: is an Earth Observation mission launched jointly by NASA and USGS that represents the world's longest continuously acquired collection of space-based moderate-resolution land remote sensing data (USGS).
Multispectral: dataset that combines data with different wavelength ranges across the electromagnetic spectrum.
Phytgeography: branch of botany that studies the geographical distribution of vegetation.
Pixel: is the basic unit of programmable color on a computer display or in a computer image.
RGB: normal color visualization using red, green and blue color combination.

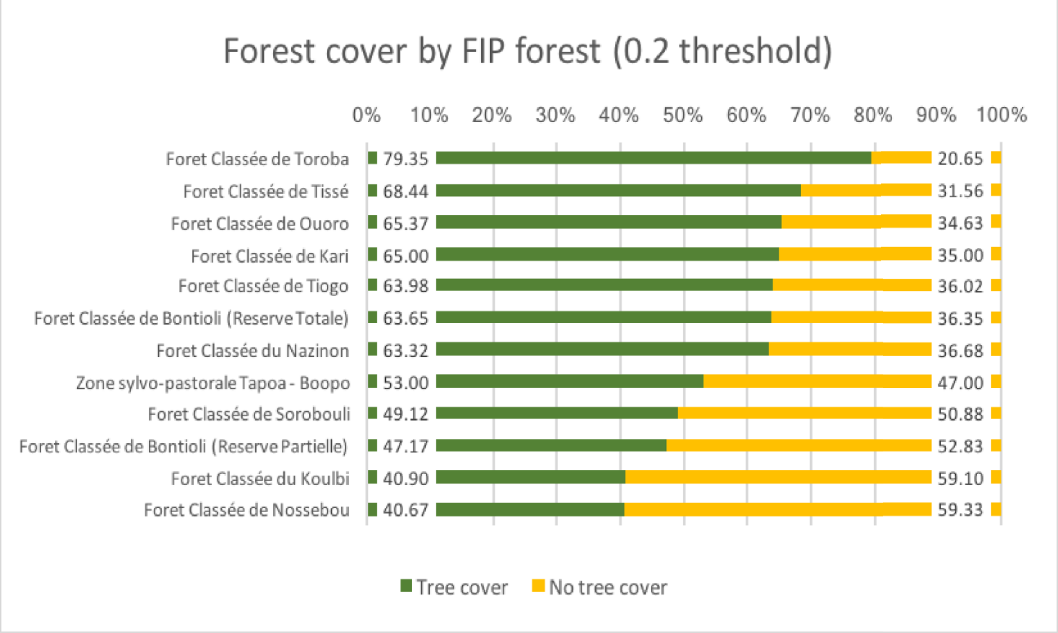

Fig. 9. Forest cover by gazetted forest for 0.2 threshold.

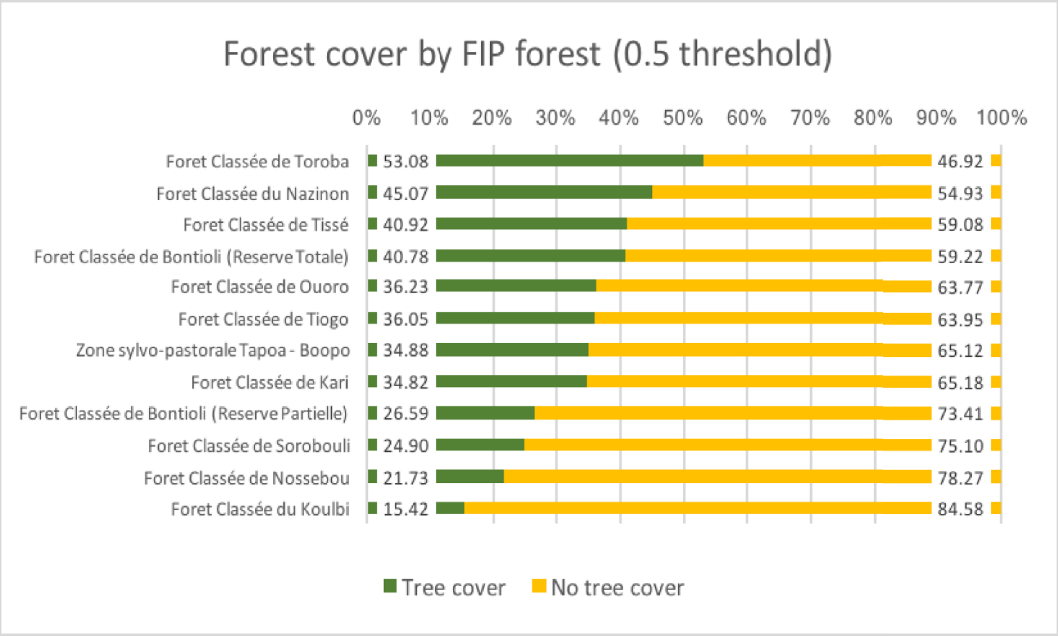

Fig. 10. Forest cover by gazetted forest for 0.5 threshold.

TIFF: a tagged image file format (known as TIF or TIFF) is a computer file that stores georeferenced raster images for analysis and visualization.

Top of atmosphere: is mainly used to help mathematically quantify Earth science parameters because it serves as an upper limit on where physical and chemical interactions may occur with molecules in the atmosphere (NASA).

Tree canopy: refers to the upper layer or habitat zone, formed by one or a group of mature tree crowns that are identified as rounded shapes from the air.

Conflict of interest

Authors declare no conflict of interest.

References

African Development Bank Group, 2013. Gazetted Forests Participatory Management Project for REDD + (GPFC/REDD+). https://www.afdb.org/fileadmin/uploads/afdb/Documents/Burkina_Faso_-_Gazetted_Forests_Participatory_Management_Project_for_REDD__PGFC-REDD__-_Appraisal_Report.pdf.

Bastin, J., Berrahmouni, N., Grainger, A., M.D. Mollicone, D., Moore, R., Patriarca, C., Picard, N., Sparrow, B., Abraham, E.M., Aloui, K., Atesoglu, A., Attore, F., Bassullu, C., Bey, A., Garzuglia, M., Garcia Montero, L.G., Mamane, B., Marchi, G., Patterson, P., Rezende, M., Ricci, S., Salcedo, I., Sanchez-Paus Diaz, A., Stolle, F., Surappaeva, V., Castro, R., 2017. The extent of forest in dryland biomes. Science 356, 635–638.

Belgiu, M., Csillik, O., 2018. Sentinel-2 cropland mapping using pixel-based and object-based timeweighted dynamic time warping analysis. Rem. Sens. 204, 509–523.

Belgiu, M., Dragut, L., 2016. Random forest in remote sensing: a review of applications and future directions. ISPRS J. Photogrammetry Remote Sens. 114, 24–31.

Blankespoor, B., Dasgupta, S., Wheeler, D., 2017. Protected areas and deforestation: new results from high-resolution panel data. Nat. Resour. Forum 41, 55–68. https://doi.org/10.1111/1477-8947.12118.nRF-OA-May-2016-0077.R1.

Bognounou, F., Tigabu, M., Savadogo, P., Thiombiano, A., Boussim, I., Oden, P., Guinko, S., 2010. Regeneration of five combretaceae species along a latitudinal gradient in sahelo-sudanian zone of Burkina Faso. Ann. For. Sci. 3, 306.

Breiman, L., 2001. Random forests. Mach. Learn. 45, 5–32.

Canadell, J.G., Gullison, R.E., Frumhoff, P.C., Field, C.B., Nepstad, D.C., Hayhoe, K., Avissar, R., Curran, L.M., Friedlingstein, P., Jones, C.D., Nobre, C., 2007. Tropical forests and climate policy. Science 316, 985–986.

Churches, C.E., Wampler, P.J., Sun, W., Smith, A., 2014. Evaluation of forest cover estimates for Haiti using supervised classification of landsat data. Int. J. Appl. Earth Obs. Geoinf. 30, 203–216.

Climate Investment Funds, 2014. Forest Investment Program. Burkina Faso. https://www.climateinvestmentfunds.org/sites/default/files/Burkina_Faso_FIP_Fact_Sheet_01-28-14.pdf.

Cutler, A., Cutler, D.R., Stevens, J.R., 2012. Random Forests. Springer US, Boston, MA, pp. 157–175. https://doi.org/10.1007/978-1-4419-9326-7_5.

Davison, A., Wang, S., Wilmshurst, J., 2006. Remote sensing of grassland-shrubland vegetation water content in the shortwave domain. Int. J. Appl. Earth Obs. Geoinf. 8, 225–236.

European Space Agency, 2015. Sentinel-2 User Handbook. https://sentinel.esa.int/documents/247904/685211/Sentinel-2_User_Handbook.

European Space Agency, 2017. Sentinel-2. http://www.esa.int/Our_Activities/Observing_the_Earth/Copernicus/Sentinel-2.

Feng, P., Wang, B., Liu, D.L., Xing, H., Ji, F., Macadam, I., Ruan, H., Yu, Q., 2018. Impacts on rainfall extremes on wheat yield in semi-arid cropping systems in eastern Australia. Climatic Change 147, 555–569.

Fisher, J.R.B., Acosta, E.A., Dennedy-Frank, J., Kroeger, T., Boucher, T., 2017. Impact of Satellite Imagery Spatial Resolution on Land Use Classification Accuracy and Modeled Water Quality. Remote Sensing in Ecology and Conservation.

Fontès, J., Guinko, S., 1995. Carte de la végétation et de l'occupation du sol (Burkina Faso). Note explicative. Laboratoire d'Ecologie Terrestre, Institut de la Carte Internationale de la Végétation. CNRS, Université de Toulouse III (France)/Institut du Développement Rural, Faculté des Sciences et Techniques, Université de Ouagadougou, Burkina Faso.

Gao, B., 1999. Ndwi—a normalized difference water index for remote sensing of vegetation liquid water from space. Remote Sens. Environ. 3, 257–266.

Garroutte, E.L., Hansen, A.J., Lawrence, R.L., 2016. Using ndvi and evi to map spatiotemporal variation in the biomass and quality of forage for migratory elk in the greater yellowstone ecosystem. Rem. Sens. 8.

Glenn, E.P., Huete, A.R., Nagler, P.L., Nelson, S.G., 2008. Relationship between remotely-sensed vegetation indices, canopy attributes and plant physiological processes: what vegetation indices can and cannot tell us about the landscape. Sensors 4, 2136–2160.

Global Forest Observation Initiative, 2014. http://www.gfoi.org/.

Goldblatt, R., Burney, J., Rivera-Ballesteros, A., 2017. High spatial resolution visual band imagery outperforms medium resolution spectral imagery for ecosystem assessment in the semi-arid brazilian sertao. Rem. Sens. 9, 1–26.

Goldblatt, R., You, W., Hanson, G., Khandelwal, A., 2016. Detecting the boundaries of urban areas in India: a dataset for pixel-based image classification in google earth engine. Rem. Sens. 634, 1–28.

Griscom, B.W., Adams, J., Ellis, P.W., Houghton, R.A., Lomax, G., Miteva, D.A., Schlesingere, W.H., Shoch, D., Siikamakig, J.V., Smith, P., Woodbury, P., Zganjar, C., Blackman, A., João Campari, R.T.C., Delgado, C., Elias, P., Gopalakrishna, T., Hamsik, M.R., Herrero, M., Kiesecker, J., Landis, E., Laestadius, L., Leavitt, S.M., Minnemeyer, S., Polasky, S., Potapovp, P., Putzq, F.E., Sanderman, J., Silvius, M., Wollenberg, E., Fargione, J., 2017. Protected areas and deforestation: new results from high-resolution panel data. Nat. Clim. Solut. 114, 11645–11650. www.pnas.org/cgi/doi/10.1073/pnas.1710465114.

Hansen, M.C., Roy, D.P., Lindquist, E., Adusei, B., Justice, C.O., Alstatt, A., 2007. A Method for Integrating Modis and Landsat Data for Systematic Monitoring of Forest Cover and Change in the congo Basin. Science Direct.

Hansen, M.C., Potapov, P.V., Moore, R., Hancher, M., Turubanova, S.A., Tyukavina, A., Thau, D., Stehman, S.V., Goetz, S.J., Loveland, T.R., Kommareddy, A., Egorov, A., Chini, L., Justice, C.O., Townshend, J.R.G., 2013. High-resolution global maps of 21st-century forest cover change. Science 342, 850–853.

Huete, A., Justice, C., Liu, H., 1994. Development of vegetation and soil indices for modis-eos. Remote Sens. Environ. 49, 224–234.

Huete, A.R., Liu, H.Q., Batchily, K., van Leeuwen, W.J.D., 1997. A comparison of

vegetation indices over a global set of tm images for eos-modis. Rem. Sens. 59, 440–451.
Huete, A.R., Obata, K., Miura, T., Yoshioka, H., 2013. Derivation of a modis-compatible enhanced vegetation index from visible infrared imaging radiometer suite spectral reflectances using vegetation isoline equations. J. Appl. Remote Sens. 1.
Karlson, M., Ostwald, M., Reese, H., Sanou, J., Tankoano, B., Mattson, E., 2015. Mapping tree canopy cover and aboveground biomass in sudano-sahelian woodlands using landsat 8 and random forest. Rem. Sens. 7, 10017–10041.
Kawamura, M., Jayamanna, S., Tsujiko, Y., 1996. Relation between social and environmental 499 conditions in colombo Sri Lanka and the urban index estimated by satellite remote 500 sensing data. Int. Arch. Photogramm. Remote Sens. 31, 321–326.
Kim, D.H., Sexton, J.O., Noojipady, P., Huang, C., Anand, A., Channan, S., Feng, M., Townshend, J.R., 2014. Global, landsat-based forest-cover change from 1990 to 2000. Remote Sens. Environ. 155, 178–193. https://doi.org/10.1016/j.rse.2014.08.017.
Kumar, Y., Sahoo, G., 2012. Analysis of parametric and non parametric classifiers for classification technique using weka. I.J. Inf. Technol. Comput. Sci. 7, 43–49.
Lanzi, P.L., Stolzmann, W., Wilson, S.W., 2018. Learning Classifier Systems: from Foundations to Applications, vol. 204 Springer-Verlag Berlin Heidelberg.
McRoberts, R.E., Liknes, G., Domke, G.M., 2014. Using a remote sensing-based, percent tree cover map to enhance forest inventory estimation. For. Ecol. Manag. 331, 12–18.
Ministry of the Environment and Sustainable Development, Government of Burkina Faso, 2012. Readiness Preparation Plan for Redd. https://www.forestcarbonpartnership.org.
Mitchard, E., Viergever, K., Morel, V., Tipper, R., 2015. Assessment of the accuracy of university of maryland (hansen et al.) forest loss data in 2 icf project areas – component of a project that tested an icf indicator methodology. https://ecometrica.com/wp-content/uploads/2015/08/UMD_accuracy_assessment_website_report_Final.pdf.
Morlini, I., 2006. On multicollinearity and concurvity in some nonlinear multivariate models. Stat. Methods Appl. 15, 3–26.
Morton, D.C., Nagol, J., Carabajal, C.C., Rosette, J., Palace, M., Cook, B.D., Vermote, E.F., Harding, D.J., North, P.R., 2014. Amazon forests maintain consistent canopy structure and greenness during the dry season. Nature 506, 221–224.
Nabuurs, G.e.a., 2007. Forestry. In: Metz, B., Davidson, O.R., Bosch, P.R., Dave, R., Meyer, L.A. (Eds.), Climate Change 2007: Mitigation of Climate Change. Contributions of Working Group III to the Fourth Assessment Report of the Intergovernmental Panel on Climate Change. Cambridge University Press, New York (chapter 9).
Pesaresi, M., Corbane, C., Julea, A., Florczyk, A.J., Syrris, V., Soille, P., 2016. Assessment of the added-value of sentinel-2 for detecting built-up area. Rem. Sens. 8, 299.
Puletti, N., Chianucci, F., Castaldi, C., 2018. Use of sentinel-2 for forest classification in mediterranean environments. Ann. Silvicultural Res. 42, 32–38.
Rodriguez-Galiano, V.F., Rigol-Sanchez, J.P., Ghimire, B., Rogan, J., Chica-Olmo, M., 2012. An assessment of the effectiveness of a random forest classifier for land-cover classification. ISPRS J. Photogrammetry Remote Sens. 67, 93–104.
Saleska, S.R., Didan, K., Huete, A.R., da Rocha, H.R., 2007. Amazon forests green-up during 2005 drought. Nature 318, 612.
Stern, N.H., 2007. The Economics of Climate Change: the Stern Review. Cambridge University press.
Tsendbazar, N.E., Herold, M., Arino, O., 2014. Global land cover mapping: current status and future trends. Remote sensing and digital image processing. In: In: Manakos, I., Braun, M. (Eds.), Land Use and Land Cover Mapping in Europe, vol. 18 Springer (chapter 2).
United States Geological Survey, 2016. West Africa: Land Use and Land Cover Dynamics, the Republic of burkina faso. https://eros.usgs.gov/westafrica/country/republic-burkina-faso.
United States Geological Survey, 2017. Sentinel-2 Multispectral Instruments (Msi). https://eros.usgs.gov/sentinel-2.
University of Maryland, 2015. Global Forest Change 2000–2014. http://earthenginepartners.appspot.com/science-2013-global-forest/download_v1.2.html.
Wang, N., Zeng, N., Zhu, W., 2010. Sensitivity, specificity, accuracy, associated confidence interval and roc analysis with practical sas implementations. In: Northeast SAS User Group Proceedings, Section of Health Care and Life Sciences, pp. 1–9.
Zha, Y., Gao, J., Ni, S., 2013. Use of normalized difference built-up index in automatically mapping urban areas from tm imagery. Int. J. Rem. Sens. 3, 583–594.